DOI: https://doi.org/10.53256/COSE_240105

Application of Remote Sensing in the Design and Monitoring of Coastal Structures

I. Petković[a], N. Šuput[b], I. Žigo[c], N. Krvavica[a], I. Ružić[a]
[a] *University of Rijeka, Faculty of Civil Engineering, Croatia*
[b] *BSK Commerce d.o.o., Croatia*
[c] *MareCon d.o.o., Croatia*

[*] *Corresponding author: ipetkovic@uniri.hr*

ABSTRACT: Evolving coastal hazards require survey methods that are rapid, accurate, and cost-efficient. This study presents a field-tested, RTK-anchored multisensor workflow that integrates Unmanned Aerial Vehicle (UAV) and handheld Structure-from-Motion (SfM) photogrammetry, smartphone LiDAR (sLiDAR), and terrestrial laser scanning (TLS) to generate engineering-grade point clouds of rubble-mound breakwaters. All datasets are co-registered within a unified control network, quality-controlled, and processed to extract key geometric parameters, including berm width, crown elevation, and cross-sectional profiles. Hybrid uncertainty is quantified by combining M3C2 normal-direction distances with alignment root-mean-square residuals to derive a 95% level of detection (LoD95), enabling robust centimetre-scale change detection. The proposed workflow is demonstrated at two Adriatic sites representative of common breakwater typologies. At the Pećine municipal breakwater, overlapping datasets are analysed using M3C2 comparison and transverse profiles to assess internal consistency and method-specific performance. At the Marina Mitan composite breakwater, transverse and longitudinal profiles derived from handheld SfM and sLiDAR are directly compared with design documentation to evaluate as-built compliance. Across both sites, sLiDAR effectively resolves undercuts and porous interior features that are partially occluded in image-based datasets, while aerial and handheld SfM provide rapid, high-density coverage in accessible and well-lit areas. TLS delivers a highly accurate reference dataset where safe access and instrument placement are feasible, albeit with greater logistical effort.The results highlight the growing importance of remote sensing techniques in contemporary coastal engineering practice and support their broader application across the design, construction, and maintenance phases of coastal infrastructure. By providing a reproducible framework for data acquisition, co-registration, and uncertainty assessment, this study reduces barriers related to processing complexity and initial investment, thereby enabling operational monitoring of critical coastal structures.

KEYWORDS: Rubble-mound breakwaters, Structure-from-Motion, Smartphone LiDAR, Photogrammetry, M3C2

1 INTRODUCTION

The increasing frequency and severity of coastal hazards driven by sea-level rise, storm intensification, and human interventions have underscored the need for rapid, accurate, and cost-effective surveying of coastal infrastructure. Traditional approaches, such as total station surveys, manual levelling, and classical aerial photogrammetry, require extensive field campaigns, specialised equipment, and skilled operators, which can limit spatial coverage and monitoring frequency (Campbell and Wynne, 2011; Wang, 2009). As coastal structures age and the impacts of extreme events intensify, engineering practice increasingly benefits from innovative methods that deliver high-quality three-dimensional (3D) information with reduced logistical effort and cost (James et al., 2013).

Recent advances in remote sensing (RS) have enabled detailed 3D mapping and structural assessment across complex coastal environments. Structure-from-Motion (SfM) photogrammetry reconstructs dense point clouds from overlapping

imagery acquired by unmanned aerial vehicles (UAVs) and handheld cameras. It routinely achieves centimetre-level accuracy and is well suited for monitoring coastal morphodynamics, including beach profiles, cliff erosion, and the geometry of breakwaters (Ružić et al., 2014, 2019; Tadić et al., 2022; Petković, 2023). Light Detection and Ranging (LiDAR) provides direct range measurements capable of capturing fine-scale surface detail and has been widely applied to extract precise geometry and detect small-scale changes in rubble-mound structures (Puente et al., 2014). More recently, the growing availability of smartphone-based LiDAR (sLiDAR) has extended data acquisition to confined and porous zones that are difficult to survey using aerial imagery or terrestrial laser scanning (TLS), thereby complementing both SfM and TLS in coastal applications (Błaszczak-Bąk et al., 2023; Syafie et al., 2024; Šuput, 2023).

This study advances current practice by integrating multiple RS platforms within a single Real-Time Kinematic (RTK)-referenced workflow for surveying rubble-mound breakwaters. The proposed workflow combines UAV-based SfM, handheld SfM, TLS, and sLiDAR, and provides practical guidance for both field acquisition and data processing using readily available hardware and commonly employed software. A unified RTK-anchored control network supports the co-registration of all datasets, after which point clouds are aligned, quality-controlled, and sectioned to extract key engineering parameters such as berm width, crown elevation, and cross-sectional geometry. Uncertainty propagation within the hybrid point clouds is explicitly addressed: normal-direction distances derived from the Multiscale Model-to-Model Cloud Comparison (M3C2) algorithm are combined with the root-mean-square (RMS) alignment residuals to estimate hybrid uncertainty and derive a Level of Detection at the 95% confidence level (LoD95), which frames all reported differences.

The proposed approach is demonstrated at two Adriatic sites representing common breakwater typologies. At the Pećine municipal breakwater, overlapping datasets are compared using M3C2 analysis and transverse profiles to assess internal consistency and method-specific performance. At the Marina Mitan composite breakwater, transverse and longitudinal profiles derived from handheld SfM and sLiDAR are directly compared with design documentation to evaluate as-built compliance. Across both sites, sLiDAR proves effective in capturing undercuts and porous regions that are partially occluded in image-based datasets, while aerial and handheld SfM provide rapid coverage and high point densities in accessible, well-lit areas.

2 STUDY AREAS AND MATERIALS

2.1 Research area

Two study sites were investigated in this work. The first site is the Pećine breakwater, located along the Pećine coastline in the city of Rijeka, Croatia (regional location in Fig. 1a; UAV view in Fig. 1b). The Pećine area is characterised by a rocky coastline with a series of small coves and pocket beaches.

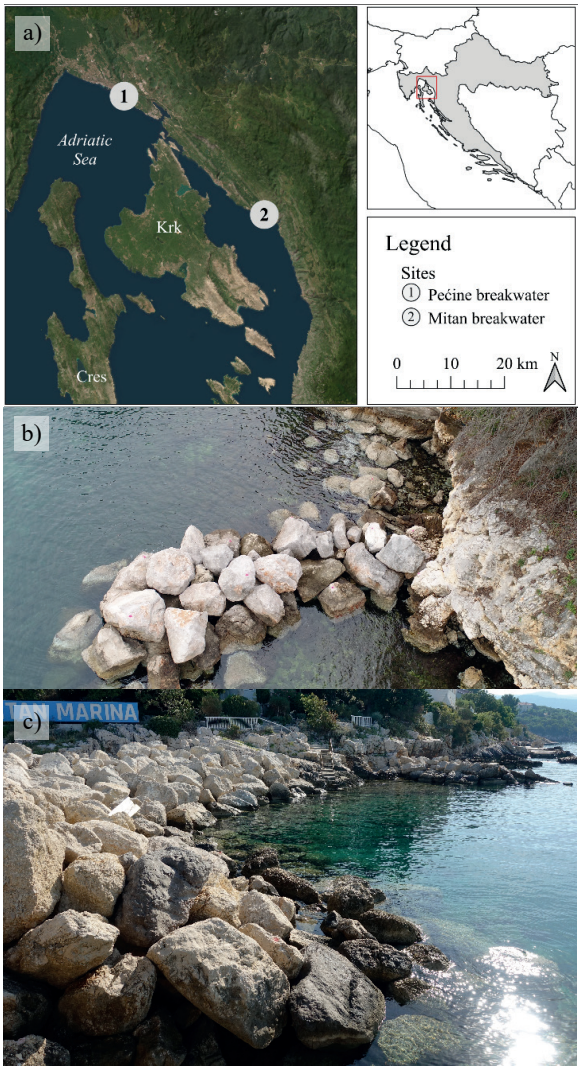

Figure 1. Study area and breakwater sites.
a) Regional location of the two investigated breakwaters on the northern Adriatic coast, showing the Pećine breakwater (site 1) in Rijeka and the Mitan breakwater (site 2) in Novi Vinodolski (basemap: ESRI World Imagery).
b) Secondary rubble-mound Pećine breakwater (site 1).
c) Rubble-mound Mitan breakwater (site 2).

The analysed segment corresponds to Crnej Beach, situated immediately adjacent to the entrance of the Pećine small municipal harbour. This study focuses on a secondary breakwater within the municipal harbour, constructed at a later stage as a simple rubble-mound structure approximately 12 m in length to mitigate wave agitation within the harbour basin. This structure is hereafter referred to as the *Pećine breakwater*.
The second study area is the rubble-mound section of a composite breakwater located at the south-eastern corner of Marina Mitan, in the city of Novi Vinodolski (regional location in Fig. 1a; shoreline photograph in Fig. 1c), hereafter referred to as the *Mitan breakwater*. The Mitan breakwater extends approximately 25 m in each direction and has an above-sea-level width of about 7 m. This structure was selected due to its representative geometry and good accessibility, providing an opportunity to assess the applicability of remote sensing (RS) methods to a commonly encountered breakwater typology.

2.2 Survey equipment

To conduct a comprehensive geometric survey of coastal structures, five complementary components were integrated into a cohesive workflow to leverage their individual strengths. The survey began with a FARO Focus3D X 130 terrestrial laser scanner (TLS), which provides millimetre-level accuracy and high-density point clouds, capturing fine surface details and precise armour-unit placement. These data form a detailed geometric baseline of the exposed armour layer.
Building on this static reference framework, a DJI Phantom 4 Advanced unmanned aerial vehicle (UAV) was employed to extend spatial coverage into broader, hard-to-access areas. The UAV acquires high-overlap aerial imagery, effectively bridging gaps in regions shadowed or occluded from ground-based scanning.
To address undercut features and interstitial voids beyond the reach of both TLS and UAV photogrammetry, smartphone LiDAR (sLiDAR) data were collected using an Apple iPhone 13 Pro. This system provides close-range depth measurements with centimetre-scale precision, enabling the infilling of localized gaps within the point cloud.
Handheld photogrammetry, performed using a Sony RX100 Mark V camera, offered flexible, high-resolution data acquisition and proved particularly effective on textured surfaces and partially occluded rock faces. This method requires minimal operator training and enriches the dataset with colour and material information that range-only sensors cannot capture.
Finally, a GNSS–RTK system ensured sub-decimetre positional accuracy across all measurements, allowing UAV-derived models, TLS point clouds, sLiDAR scans, and handheld Structure-from-Motion (SfM) reconstructions to be co-registered within a single, unified coordinate framework.

3 METHODOLOGY

3.1 Data acquisition

Field campaigns were conducted on three occasions (two at Crnej and one at Mitan) to acquire high-resolution three-dimensional (3D) data of two rubble-mound breakwaters. A unified georeferencing procedure was implemented at all sites. High-contrast ground control targets (painted panels and spray-painted markers) were distributed around the perimeter and across accessible surfaces, and a GNSS–RTK survey was then used to record centimetre-level coordinates for each ground control point (GCP). This established a rigid control network for the subsequent co-registration of all datasets.
Following the establishment of the GCP network, multisensor data acquisition was carried out according to site-specific conditions. Static terrestrial laser scanning (TLS) was employed where unobstructed vantage points allowed the capture of dense 3D point clouds. Unmanned aerial vehicle (UAV) flights provided overlapping oblique imagery for Structure-from-Motion (SfM) photogrammetric reconstruction, while handheld devices—smartphone LiDAR (sLiDAR) and a digital camera—were used to document undercut sections, overhangs, and confined spaces inaccessible to TLS or UAV platforms. All point clouds and image datasets were referenced to the same control network and co-registered to produce unified, high-fidelity site models.

3.1.1 Pećine breakwater survey

Data were collected under overcast, low-wind conditions to minimise shadows and surface ripples (Table 1 summarises the acquisition dates, platforms, and settings). The first campaign (February 2023) combined TLS using a FARO Focus3D X 130 with three tripod stations positioned around the site (three scans acquired in approximately 30 min). As the breakwater lay at the edge of the mapped area, the landward side was not fully captured. A concurrent UAV survey was conducted using a DJI Phantom 4 Advanced, which flew low-altitude oblique paths at

approximately 45° for 15 min, acquiring 220 images for SfM reconstruction.

To document undercuts and a small coastal cave along the breakwater face, smartphone LiDAR (iPhone 13 Pro) was operated at close range. A second campaign (June 2023) employed handheld SfM using a Sony RX100 Mark V camera; 340 overlapping photographs were acquired from multiple land-based viewpoints over approximately 30 min, covering the structure from the base to the crown.

All datasets were georeferenced to the common GNSS–RTK control network and subsequently co-registered into a single, high-resolution 3D model of the Pećine breakwater.

Table 1. Acquisition details for the Pećine breakwater surveys.

Survey No.	Date	Method and equipment
1	21.02.2023	SfM (UAV) DJI Phantom 4 Advanced
1	21.02.2023	TLS Focus3D X 130
1	21.02.2023	sLiDAR iPhone 13 Pro
2	30.06.2023	SfM handheld Sony RX100 Mark V

3.1.2 Marina Mitan breakwater survey

On 11 September 2023, a ground control network was established across the Marina Mitan breakwater and surveyed using GNSS–RTK. Under clear and calm weather conditions, handheld Structure-from-Motion (SfM) photogrammetry was carried out using a Sony RX100 Mark V camera. A total of 540 overlapping photographs were acquired over approximately 1 hour, with an overlap of at least 60%, covering the structure from the base to the crown. In parallel, smartphone LiDAR (sLiDAR; iPhone 13 Pro) was operated at close range to capture the interior geometry through accessible voids within the armour layer.

The approximately 30 m long rubble-mound section was selected as a test site to evaluate the effectiveness of sLiDAR as a complementary technique to handheld SfM photogrammetry. Following data acquisition, all ground control points were re-measured using GNSS–RTK to verify positional integrity. The handheld SfM imagery and sLiDAR point cloud were then referenced to the same control network and co-registered into a unified spatial dataset.

The methods and equipment used for Survey 3 at the Marina Mitan breakwater are summarised in Table 2.

Table 2. Acquisition details for the Marina Mitan breakwater survey.

Survey No.	Date	Method and equipment
3	11.09.2023	sLiDAR iPhone 13 Pro
3	11.09.2023	SfM (handheld) Sony RX100 Mark V

3.2 Data processing

This section outlines the data-processing workflow applied to all datasets. Imagery acquired using UAV- and handheld-based Structure-from-Motion (SfM), terrestrial laser scanning (TLS) data, and smartphone LiDAR (sLiDAR) point clouds were imported into dedicated software environments for preprocessing and georeferencing. All outputs were referenced to the same GNSS–RTK control network to ensure spatial consistency.

All SfM photographs were processed using Agisoft Metashape (v1.8). Image quality was evaluated using the Estimate Image Quality tool, and frames with quality scores below 0.50 were excluded, in accordance with the software documentation and established best practices (Agisoft, 2021; Over et al., 2021). UAV images, which include approximate camera positions stored in EXIF metadata, were aligned using the Reference Preselection option, while handheld images without geotags were aligned using the High Accuracy preset.

Following initial alignment, low-confidence tie points—characterized by a low number of observations and high reprojection errors—were removed through Gradual Selection and manual inspection. Dense point clouds were subsequently generated using the High quality setting, resulting in approximately 3–7 million points per breakwater (UAV-derived point cloud shown in Fig. 2; handheld SfM-derived point cloud shown in Fig. 3).

Ground control coordinates for 11 targets, obtained from the GNSS–RTK survey and referenced to the HTRS96 / Croatia TM coordinate system (EPSG:3765), were imported into the project, manually marked, and used to refine model scale and orientation. The final

alignment to the control network achieved centimetre-level accuracy.

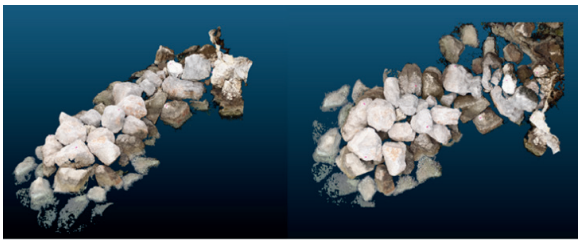

Figure 2. UAV-SfM 3D point cloud of the Pećine breakwater generated in Agisoft Metashape.

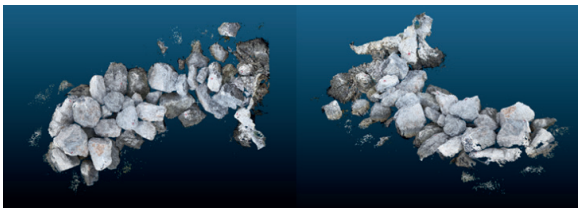

Figure 3. Handheld SfM 3D point cloud of the Pećine breakwater generated in Agisoft Metashape.

To generate a 3D point cloud of the Pećine breakwater using terrestrial laser scanning (TLS), data acquired with the FARO Focus3D X 130 were processed in FARO Scene (v2019). Noise filtering was enabled (Filter Stray Scan Points, grid size: 3 px, distance threshold: 0.02 m), and the resolution was set to Fine (corresponding to a point spacing of 1.56 mm at a range of 10 m) (FARO Technologies Inc., 2015). Three scan stations were registered using the instrument's onboard orientation sensors to preserve relative pose. Because the rubble-mound structure was only partially accessible, the TLS survey captured the seaward face of the breakwater and the adjacent Crnej Beach, while the landward face and crest were incompletely surveyed (Fig. 4). Consequently, full surface meshing of the structure was not attempted.

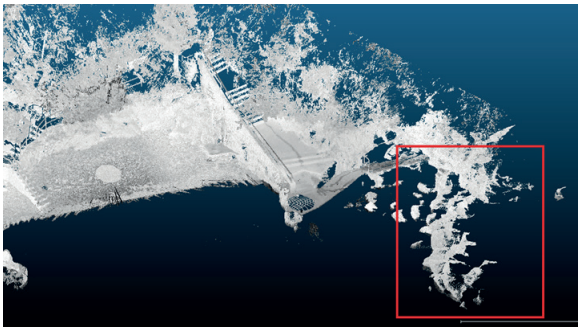

Figure 4. Partial TLS point cloud of the Crnej Beach area processed in CloudCompare, showing points captured from one side of the Pećine breakwater structure (highlighted in red).

The Mitan breakwater was surveyed in three segments using the Scaniverse application on an iPhone 13 Pro. The main segment covered approximately 30 m of the structure, while two auxiliary segments ranged between 5 and 10 m in length. Following device-side processing, the point clouds were exported and imported into CloudCompare for georeferencing and cross-section extraction (CloudCompare Wiki, 2023) (Fig. 5).

Figure 5. Segment of the Mitan breakwater point cloud acquired using sLiDAR scanning.

All point clouds and image-derived models were referenced to the same GNSS–RTK control network and subsequently rigidly aligned and quality-checked prior to analysis. The following sections describe the quantification of overlap uncertainty—combining M3C2 normal-direction distances with alignment root-mean-square (RMS) values—and the extraction of engineering cross-sections.

3.3 Error propagation in hybrid point clouds

Uncertainty in multi-sensor point cloud overlaps was quantified in CloudCompare by combining the alignment RMS of registration residuals with surface-normal distances computed using the Multiscale Model to Model Cloud Comparison (M3C2) algorithm (Lague et al., 2013). Registration was performed using point-pair matching followed by Iterative Closest Point (ICP) alignment. The alignment RMS represents the root mean square of closest-point residuals after rigid registration and is reported in metres.

M3C2 computes normal-direction distances by estimating local surface normals via principal component analysis using a diameter of $D = 0.03$ m. A normal-aligned projection cylinder (projection diameter: 0.05 m; maximum depth: 0.50 m) is then used to identify neighbouring points from both point clouds. These neighbours are projected onto the normal direction, and the mean positions μ_1 and μ_2 are calculated for the reference and compared clouds, respectively.

Their difference defines the signed separation distance d (Eq. 1):

$$d = \mu_2 - \mu_1 \quad (1)$$

Two quality metrics were evaluated for each core point: the number of supporting points in each cloud ($N_{pts1,2}$) and the local surface roughness ($STD_{1,2}$). Statistical summaries were computed for a high-confidence subset defined by $N_{pts1,2} \geq 20$, $STD_{1,2} \leq 0.05$ m, and an analysis window $|d| \leq 0.01$ m (coverage statistics are additionally reported for $|d| \leq 0.03$ m). The relative dispersion σ_{rel} was calculated as the standard deviation of d within this subset.

The hybrid uncertainty σ_{hyb} was then defined according to Eq. (2), where σ_{reg} denotes the alignment RMS:

$$\sigma_{hyb} = \sqrt{\sigma_{rel}^2 + \sigma_{reg}^2} \quad (2)$$

The minimum detectable change at the 95% confidence level, also referred to as the Level of Detection (LoD95), was subsequently derived (Eq. 3), following established practice in M3C2-based change detection (James et al. 2017; Winiwarter et al. 2021; Lague et al. 2013).

$$LoD_{95} = 1.96\sigma_{hyb} \quad (3)$$

3.4 Extraction of Point-Cloud Cross-Sections

Cross-sections were extracted from the merged point clouds of the Pećine breakwater using CloudCompare, following consistent procedures across all sensing methods. A longitudinal reference axis was first defined along the breakwater crest, after which four transverse axes were positioned at 2.5 m intervals, oriented perpendicular to the longitudinal axis. An example of the axis configuration applied to the UAV-SfM point cloud is shown in Fig. 6. Slicing the point cloud along these axes yielded narrow two-dimensional profiles through the armour layer. An example of the extracted UAV-SfM cross-sections is presented in Fig. 7.

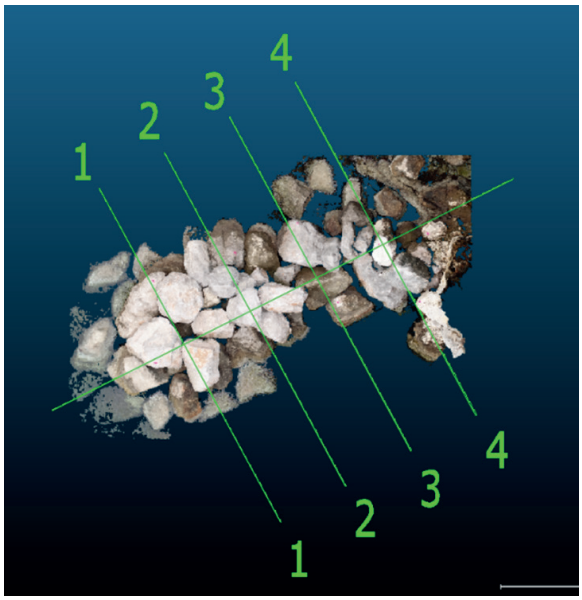

Figure 6. Example of longitudinal and transverse axes defined on the UAV-SfM point cloud of the Pećine breakwater in CloudCompare.

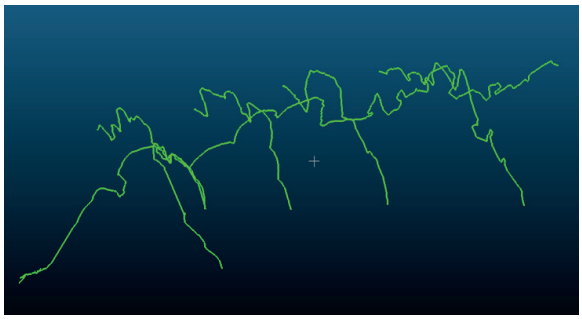

Figure 7. Example of cross-sections extracted from the UAV-SfM point cloud, showing Pećine breakwater profiles generated in CloudCompare.

For each sensing method, the extracted cross-sections—representing only the outer surface of the breakwater—were trimmed to their uppermost contours and exported as DXF polylines. These DXF files were subsequently imported into AutoCAD to remove redundant vertices and standardize line styles. The four transverse profiles derived from each method were then overlaid to enable direct geometric comparison (Fig. 8).

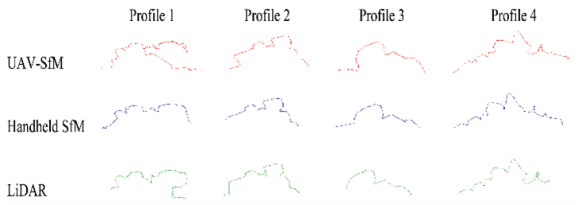

Figure 8. Four transverse cross-sections derived from UAV-SfM, handheld SfM, and sLiDAR data, exported as DXF files and edited in AutoCAD.

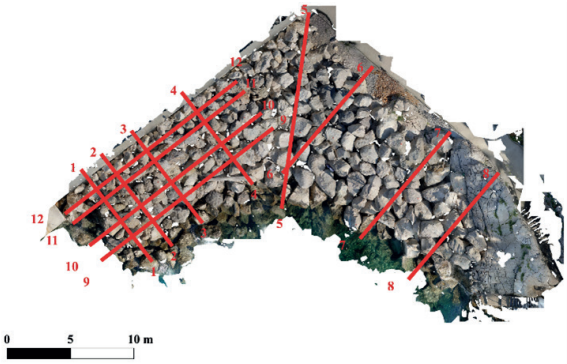

Figure 9. Selected transverse and longitudinal profiles delineated on the Mitan breakwater point cloud in AutoCAD.

Three-dimensional point clouds obtained from SfM photogrammetry and sLiDAR were also used to evaluate the as-built geometry of the Mitan breakwater against its original design documentation. Following image processing in Agisoft Metashape, selected transverse and longitudinal profiles were delineated directly on the point cloud and drafted in AutoCAD (Fig. 9).

These profiles, together with the corresponding point cloud data, were exported in ASCII format and imported into MATLAB, where custom scripts were applied to generate numerical cross-sections for both sensing techniques. The resulting profiles were subsequently reimported into AutoCAD for graphical comparison with the design drawings.

3.5 Analysis of the survey methods employed

A comparative assessment of UAV-SfM, TLS, handheld SfM, and sLiDAR was conducted at the Pećine rubble-mound breakwater. Table 3 summarises the relative direct costs, required expertise, field acquisition time, and processing effort associated with each method, using harmonised categories. The comparison provides a practical decision-support matrix for selecting appropriate survey techniques in comparable coastal engineering applications.

Table 3. Relative time, cost, effort, and expertise associated with the *survey methods applied at the Pećine breakwater* (categories *are indicative and* standardised *across* survey *campaigns*).

Method	Direct cost (relative)	Required expertise	Acquisition time (field)	Processing time (operator)
UAV–SfM[1]	Medium to Low	Moderate	Low	Moderate
Handheld–SfM[2]	Low	Low to Moderate	Medium	Moderate
sLiDAR[3]	Very Low	Low	Low	Low to Moderate
TLS[4]	High	High	Medium	High

Notes:
[1] DJI Phantom 4 Advanced; [2] Sony RX100 V; [3] iPhone 13 Pro; [4] FARO Focus3D X130.
a) Acquisition time (field): Very Low < 15 min; Low 15–30 min; Medium 30–60 min; High > 60 min.
b) Direct cost (indicative incremental per survey): Very Low: €0–€50 per day (smartphone or application already owned); Low: €20–€60 per day to rent, or approximately €500–€1,000 to purchase a consumer-grade camera; Medium to Low: €80–€200 per day to rent, or approximately €1,200–€2,500 to purchase a prosumer UAV; High: €300–€800 per day to rent, or approximately €20,000–€60,000 to purchase a TLS unit.
c) Processing effort (operator time, excluding computation): Very Low < 1 h; Low 1–2 h; Moderate 2–4 h; High > 4 h.
d) Required expertise: Low (app-guided data capture); Low to Moderate (consumer camera with basic SfM processing); Moderate (UAV operation with photogrammetric processing and GCP handling); High (survey-grade TLS deployment, scan planning, and point cloud registration).

4 RESULTS AND DISCUSSION

4.1 Quantitative Overlap Metrics and LoD95

Using the CloudCompare M3C2 algorithm, the UAV-SfM reconstruction of the Pećine breakwater was compared with the handheld SfM reconstruction. The analysis was conducted on a high-confidence subset defined by a minimum point support in both clouds of $N_{pts1,2} \geq 20$, local surface roughness $STD_{1,2} \leq 0.05$m, and a reporting filter of $|d| \leq 0.01$m. The resulting overlap quality is high.

The mean signed distance between the two datasets is effectively zero ($d = -0.00096$ m), with millimetric dispersion ($\sigma_{rel} = 0.004324$ m). The resulting hybrid uncertainty yields a level of detection at 95% confidence of $LoD_{95} = 0.02135$m. Spatial coverage is robust and

representative of the entire structure: 67.64% of all core points fall within ±1 cm ($N_{\pm 1} = 2{,}269{,}113$) and 73.59% within ±3 cm ($N_{\pm 3} = 2{,}468{,}686$) out of a total of $N_{\text{all}} = 3{,}354{,}741$, indicating close agreement over most of the breakwater.

The spatial distribution of M3C2 distances for the high-confidence subset is shown in Figure 10, with the handheld SfM point cloud used as the core dataset. Colours are clipped to ±0.01 m, and distances follow Eq. (1), such that positive values indicate that the UAV-SfM surface lies above the handheld SfM core. Residuals outside this interval are predominantly concentrated at block edges and within occluded recesses, reflecting local geometric complexity rather than systematic bias between the datasets.

From a practical engineering perspective, differences in crest elevation, berm width, or slope exceeding approximately 2–3 cm can be interpreted as real geometric variations. Smaller differences fall below the detection capability of the combined workflow unless further improvements in alignment precision are achieved.

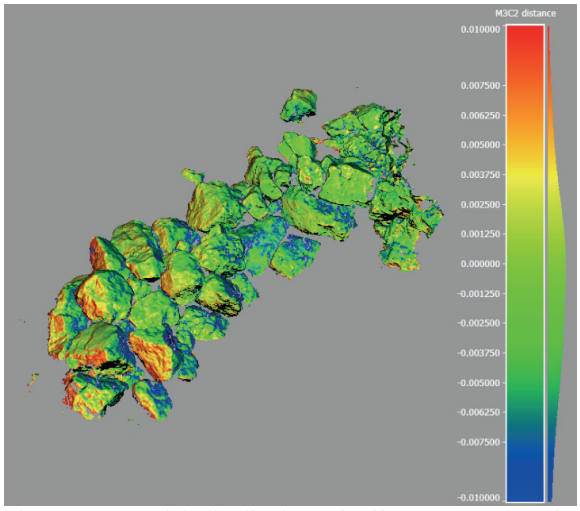

Figure 10. Spatial distribution of offsets comparing the UAV-SfM reconstruction to the handheld SfM core. Colours encode distances according to Eq. (1) and are clipped to ±0.01 m; positive values indicate the UAV-SfM surface above the core.

4.2 Cross-sectional analysis of the Pećine breakwater point clouds

The transverse cross-sections of the Pećine breakwater indicate that UAV-SfM, handheld SfM, and sLiDAR capture the overall armour-block geometry with a high degree of consistency. Figure 11 overlays Profiles 1–4 to illustrate the level of agreement between methods.

In Profile 1, the UAV-SfM trace exhibits a faint secondary line beneath the true contour, caused by oblique viewing angles that partially captured undercut block faces. A single spurious point is also present in the handheld SfM reconstruction at the same location, attributable to limited camera access between blocks. Smartphone LiDAR, although unable to resolve a small central void, provides the most complete representation in this profile due to its ease of close-range manoeuvring.

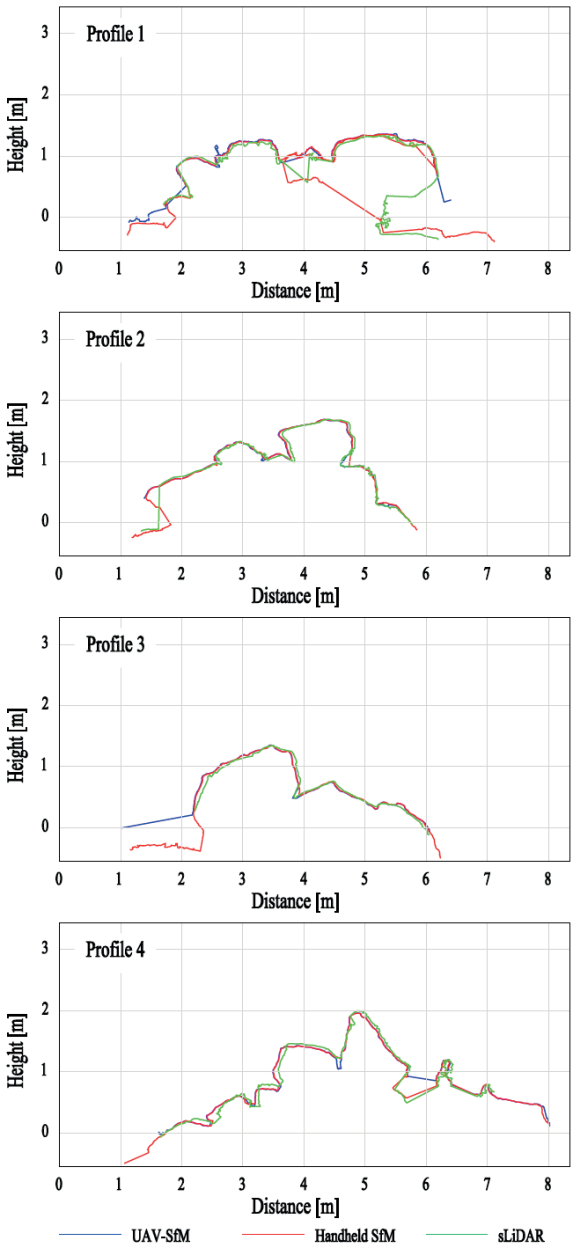

Figure 11. Overlaid transverse cross-section profiles (Profiles 1–4) of the Pećine breakwater obtained using UAV-SfM, handheld SfM, and sLiDAR, displayed in AutoCAD.

Profile 2 shows near-perfect overlap among all three methods in an unobstructed section of the structure. Profile 3 similarly demonstrates strong agreement; however, the sLiDAR profile truncates on the seaward side where water-surface reflections prevented reliable returns, whereas both SfM-based profiles extend slightly further before encountering occlusions. In Profile 4, a local deviation near the 6 m mark is evident in the handheld SfM profile, where a narrow inter-block gap was not captured and the reconstruction consequently smoothed the surface.

Overall, UAV-SfM and handheld SfM perform comparably to sLiDAR in well-lit and accessible areas, whereas sLiDAR is superior in zones characterized by undercuts, occlusions, or restricted access.

Profile-wise discrepancies relative to the sLiDAR reference were quantified using the M3C2 metric with a projection scale of 0.02 m. Across Profiles 1–4, the signed mean deviations are small (approximately 5–6 mm), while the standard deviation typically ranges between 4 and 6.5 cm, resulting in method-level root-mean-square (RMS) values of about 4.8 cm for both UAV-SfM and handheld SfM (Table 4). The largest dispersion occurs in Profile 1 for UAV-SfM (RMS ≈ 6.5 cm), consistent with the presence of local occlusions and reduced surface texture. In regions where all methods overlap, the majority of deviations fall within ±5 cm.

Table 4. M3C2 deviations (m) between SfM-derived point clouds and the sLiDAR reference for four transverse cross-sections (P1–P4) at the Pećine breakwater.

Profile	Method vs. LiDAR	Points	Mean (m)	Std. dev. (m)	RMS (m)
P1	UAV SfM – LiDAR	14,297	0.00109	0.06511	0.06512
	Handheld SfM – LiDAR	30,454	-0.0044	0.05063	0.05082
P2	UAV SfM – LiDAR	11,832	0.00953	0.04103	0.04212
	Handheld SfM – LiDAR	28,840	0.01298	0.04622	0.04801
P3	UAV SfM – LiDAR	10,950	0.00349	0.04055	0.0407
	Handheld SfM – LiDAR	21,428	0.00687	0.04716	0.04766
P4	UAV SfM – LiDAR	18,374	0.00778	0.04379	0.04448
	Handheld SfM – LiDAR	42,363	0.00945	0.04424	0.04524

4.3 Comparison of the as-built Mitan breakwater with design specifications

To evaluate conformity with the design, numerical cross-sections derived from handheld SfM and sLiDAR point clouds were compared with the project documentation (MareCon, 2023). Figure 12 presents all extracted sections in a single panel, comprising transverse Profiles 1–8 and longitudinal Profiles 9–12, with handheld SfM shown in blue and sLiDAR in red.

Within the transverse set, Profiles 2, 3, and 4 demonstrate that the sLiDAR-derived contours resolve interstitial voids between armour blocks that are only partially captured by handheld SfM, owing to the latter's reliance on sufficient image overlap. Profile 4 further illustrates a case where the sLiDAR trace terminates due to an obstructed incidence angle, whereas the handheld SfM contour extends farther owing to a greater stand-off distance. Profiles 5 and 8 exhibit incomplete sLiDAR traces associated with the segmented acquisition of the breakwater, which complicated merging and georeferencing across individual segments. Minor deviations in the handheld SfM profiles are observed in shadowed or steeply inclined areas where photographic coverage was limited.

In the longitudinal set, Profiles 9–12 closely follow the intended design elevations. Profile 12 accurately reproduces the 3 m elevation, while Profiles 11 (3 m), 10 (2 m), and 9 (1 m) similarly conform to their respective design targets. In Profile 10, the sLiDAR contour extends further down the seaward slope than the handheld SfM profile, reflecting the ability of close-range sLiDAR acquisition to capture undercut and overhanging zones. Overall, both methods produce closely overlapping contours, with deviations generally within a few centimetres across the analysed sections, indicating no systematic departures from the design geometry.

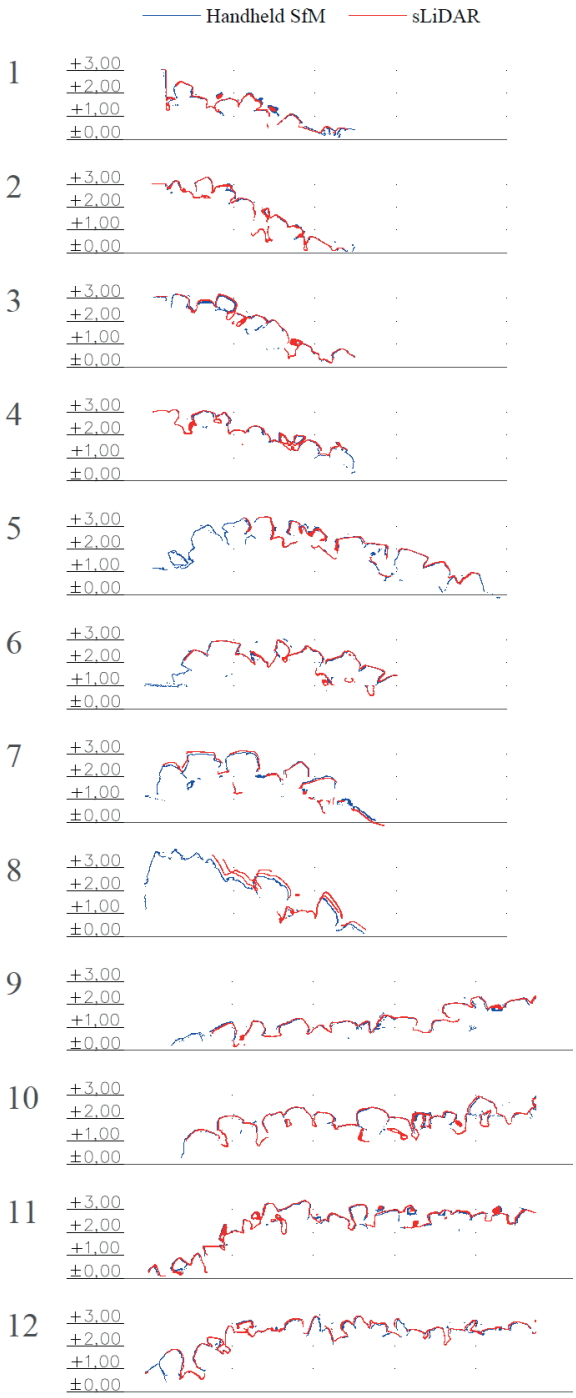

Figure 12. Cross-sections of the Marina Mitan breakwater derived from handheld SfM (blue) and sLiDAR (red) point clouds in AutoCAD. Transverse Profiles 1–8 and longitudinal Profiles 9–12 are shown, with axes in metres.

Figure 13 shows the design cross-section with the locations of longitudinal Profiles 9–12 indicated for reference. In addition, transverse Profile 2 is directly overlaid along the seaward vertical wall using the design documentation (MareCon, 2023). This profile clearly illustrates the geometry and elevation of the stone-filled armour layer, where the sLiDAR-derived contour (red) closely tracks the design line. Cross-sectional measurements yield a berm width of 2.60 m and a revetment slope of 1:1.5, confirming that the as-built structure complies with the original specifications.

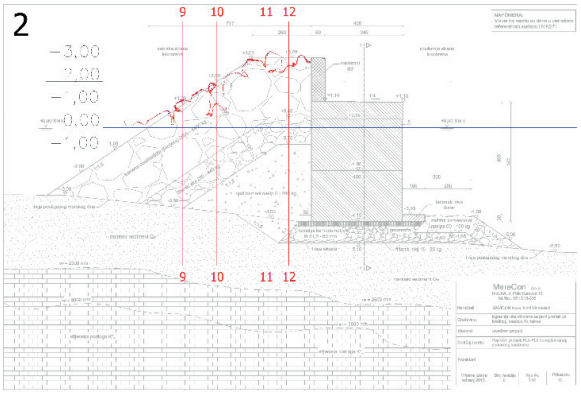

Figure 13. Point cloud cross-sections for longitudinal Profiles 9–12 and transverse Profile 2 on the Mitan breakwater, overlaid on the design section. sLiDAR (red) contours closely match the design geometry (MareCon, 2023); Profile 2 indicates a 2.60 m berm width and a 1:1.5 revetment slope.

CONCLUSIONS

This study demonstrates that a multisensor, RTK-referenced point-cloud workflow can capture and analyse the geometry of rubble-mound breakwaters with decision-grade accuracy at modest cost and operational effort. UAV-based SfM, handheld SfM, sLiDAR, and—where feasible—TLS were integrated within a single control network, then aligned, quality-checked, and analysed using consistent parameters. Uncertainty in hybrid overlaps was treated explicitly by combining M3C2 normal-direction distances with the alignment root-mean-square (RMS), yielding a hybrid uncertainty and a 95% confidence level of detection that frames all comparisons.

At the Pećine breakwater, the overlap between UAV SfM and handheld SfM is strong: the mean signed normal distance is effectively zero, with millimetric dispersion. Coverage within ±1 cm and ±3 cm of the normal direction reaches 67.64% and 73.59% of all core points

(approximately 3.35 million), respectively. The derived detection limit at 95% confidence is 0.021 m, indicating that differences on the order of two to three centimetres can be interpreted as real changes across most of the structure. Transverse cross-sections extracted at 2.5 m spacing confirm close agreement among methods; profile-wise RMS values typically range from four to five centimetres, with larger residuals confined to block edges and occluded recesses where true overlap is limited.

At the Mitan breakwater, handheld SfM and sLiDAR successfully reproduce the design elevations and dimensions. The measured berm width is 2.60 m, and the revetment slope conforms to the specified 1:1.5. The datasets are both substantial and complementary: the sLiDAR point cloud comprises approximately 10.0 million points, while the handheld SfM point cloud contains about 2.25 million points. Together, they resolve both exterior surfaces and interior voids accessible from the armour layer. Overall, the two methods produce closely overlapping contours, with no systematic departures from the design geometry.

The comparative assessment clarifies key operational trade-offs. UAV SfM provides the fastest coverage and highest point density for a given field time; handheld SfM adds colour and geometric detail in accessible areas; sLiDAR effectively resolves undercuts and interior voids at close range; and TLS offers a highly precise baseline where safe access and station placement are possible, albeit with greater deployment demands. The accompanying table summarising time, cost, effort, and expertise requirements serves as a practical decision aid for selecting a fit-for-purpose combination of methods in coastal surveys. In practice, UAV SfM is recommended for rapid, large-area surveys when time and personnel are constrained, with handheld SfM and sLiDAR added where complex geometry, shadowing, or occlusions are present.

Periodic re-survey following a consistent schedule, using the same control network and processing parameters, supports early detection of settlement, armour displacement, and toe migration. The workflow scales effectively to harbour-scale assets through a stable RTK control framework and a tiled acquisition and processing strategy, preserving uniform accuracy as spatial extent increases and enabling targeted re-survey of affected sections after storms or construction activities. Limitations arise where surfaces are not jointly observed, notably at block edges, occluded recesses, and near the waterline. These effects are mitigated by reporting results for a high-confidence subset, documenting M3C2 and cross-section extraction parameters, and prioritising robust registration. Future work should focus on improving alignment in areas with complex access, adopting adaptive neighbourhood selection for M3C2, and routinely using empirical cumulative distributions of normal distances to summarise spatial coverage and acceptance thresholds. Collectively, these steps further consolidate multisensor point-cloud workflows as a reliable basis for construction verification, condition monitoring, and targeted maintenance of coastal infrastructure.

ACKNOWLEDGEMENTS

This work was supported by the University of Rijeka through the GraDiS project “Unaprjeđenje modela stjecanja stručnih kompetencija učenjem uz rad kroz izradu diplomskog rada” (Project code A3-21-6; UNIRI CLASS A3) and by the Croatian Science Foundation (Project IP-2022-10-7598). The GraDiS project was led by Associate Professor Dr. Sc. Silvija Mrakovčić and funded under the University of Rijeka’s UNIRI CLASS A3 programme. The funding bodies provided financial support for data acquisition, analysis, and manuscript preparation but were not involved in the study design, data interpretation, writing of the manuscript, or the decision to submit it for publication.

REFERENCES

Agisoft (2021) Agisoft PhotoScan User Manual: Professional Edition, Version 1.7. Agisoft LLC.

Błaszczak-Bąk, W.; Janicka, J.; Dumalski, A.; Masiero, A. (2023). Integration of Terrestrial Laser Scanning and Smartphone LiDAR: The Case Study of Lidzbark Castle. *International Archives of the Photogrammetry, Remote Sensing and Spatial Information Sciences*, XLVIII-1/W1, 51–56.

Campbell, J. B.; Wynne, R. H. (2011). Introduction to Remote Sensing. Guilford Press.

CloudCompare Wiki (2023). *CloudCompare Wiki* [Online]. Retrieved June 19, 2023, from https://www.cloudcompare.org/doc/wiki/index.php/Main_Page

FARO Technologies Inc. (2015). FARO Laser Scanner Focus3D X 130 Manual, February 2015.

James, M.; Ilić, S.; Ružić, I. (2013). Measuring 3D Coastal Change with a Digital Camera. In Proceedings of Coastal Dynamics 2013, Arcachon, France; pp. 893–904.

James, M. R.; Robson, S.; Smith, M. W. (2017). 3-D uncertainty-based topographic change detection with structure from motion photogrammetry: Precision maps for ground control and directly georeferenced

surveys. Earth Surface Processes and Landforms, 42(12), 1769–1788.
Lague, D.; Brodu, N.; Leroux, J. (2013). Accurate 3D comparison of complex topography with terrestrial laser scanner: Application to the Rangitikei canyon (N-Z). *ISPRS Journal of Photogrammetry and Remote Sensing*, 82, 10–26. (doi:10.1016/j.isprsjprs.2013.04.009)
MareCon d.o.o. (2023). *Tehnička dokumentacija lukobrana marine Mitan*. MareCon d.o.o., Rijeka, Croatia
Over, J. R.; Ritchie, A. C.; Kranenburg, C. J.; Brown, J. A.; Buscombe, D. D.; Noble, T.; Sherwood, C. R.; Warrick, J. A.; Wernette, P. A. (2021). Processing Coastal Imagery with Agisoft Metashape Professional Edition, Version 1.6 - Structure from Motion Workflow Documentation. U.S. Geological Survey Open-File Report 2021-1039, 46 p. https://doi.org/10.3133/ofr20211039.
Petković, I. (2023). Primjena 3D oblaka točaka za projektiranje u priobalnom području [Master's thesis, University of Rijeka, Faculty of Civil Engineering]. University of Rijeka Repository.
Puente, I.; Lindenbergh, R.; González-Jorge, H.; Arias, P. (2014). Terrestrial laser scanning for geometry extraction and change monitoring of rubble mound breakwaters. *ISPRS Annals of the Photogrammetry, Remote Sensing and Spatial Information Sciences* II-5: 289–296.
Ružić, I.; Dugonjić, S.; Benac, Č.; Krvavica, N. (2019). Assessment of the Coastal Vulnerability Index in an Area of Complex Geological Conditions on the Krk Island, Northeast Adriatic Sea. Geosciences, 219(9).
Ružić, I.; Marović, I.; Benac, Č.; Ilić, S. (2014). Coastal cliff geometry derived from structure-from-motion photogrammetry at Stara Baška, Krk Island, Croatia. Geo-Marine Letters, 34(6), 555–565.
Syafie, F. S.; Khalid, N.; Tahar, K. N.; Naharudin, N.; Kamaruddin, A. H. (2024). Assessment the Accuracy of Crack Detection Derived from Smartphone LiDAR and TLS Dataset. *Proceedings of the 2024 IEEE International Conference on Automatic Control and Intelligent Systems*, 1–5.
Šuput, N. (2023). Primjena daljinskih istraživanja kod projektiranja i praćenja obalnih građevina (Master's thesis, University of Rijeka, Faculty of Civil Engineering). University of Rijeka Repository.
Tadić, A.: Ružić, I.; Krvavica, N.; Ilić, S. (2022). Post-Nourishment Changes of an Artificial Gravel Pocket Beach Using UAV Imagery. Journal of Marine Science and Engineering, 10(3).
Wang, Y. (Ed.) (2009). Remote Sensing of Coastal Environments. CRC Press.
Winiwarter, L.; Anders, K.; Höfle, B. (2021). M3C2-EP: Pushing the limits of 3D topographic point cloud change detection by error propagation. ISPRS Journal of Photogrammetry and Remote Sensing, 178, 240–258.